

Parametric Optimization and Performance Analysis of a Central Receiver Solar Power Plant: A Numerical Study for Enhanced Solar Field and Receiver

Khalid Bouaiche^{1*}, Mohammed Aymane Loulidi Lahkim¹, Abdelhak Ouassit¹, Hamid Loulijat¹

¹Faculty of Science and Technology, Mohammedia, Hassan II University, Casablanca, Morocco.

Abstract. In the context of the energy transition and the search for sustainable solutions, central receiver solar power plants have become a promising technology for generating green electricity. The present case study aims to identify the optimal dimensional parameters of a solar tower plant located in southern Morocco. Typical Meteorological Year (TMY) data were collected for the targeted region to ensure a realistic representation of local climatic conditions. The modelling of the optical behavior of the heliostat field and the receiver is carried out using a simulation approach based on the Monte Carlo Ray Tracing (MCRT) method. The main objective is to identify an optimal configuration by varying several key parameters, such as the layout of the heliostats, the tower height, and the receiver dimensions. The results obtained show that an increase in the tower height leads to a growth in the number of accessible heliostats and therefore an expansion of the mirror field. Optimal performance is achieved for a tower height between 180 and 200 meters. For this height of the tower the optical losses due to dissipation effects and atmospheric attenuation are at their maximum, reaching approximately 5.05% and 8.9%, respectively. On the other hand, losses due to blocking/shading effects and the cosine effect reach their minimum values, at approximately 1% and 20%, respectively.

Keywords: Central receiver system, Monte Carlo Ray Tracing, Optical efficiency, SolarPILOT, Renewable energy.

Nomenclature:

η_{opt}	Optical efficiency
η_{cos}	Efficiency due to cosine effect
η_{blk}	Efficiency due to blocking/shading
η_{spl}	Efficiency due to spillage (Interception)
η_{att}	Efficiency due to atmospheric attenuation
PVGIS	Photovoltaic Geographical Information System
TMY	Typical Meteorological Year
DNI	Direct Normal Irradiance (W/m^2)
CSP	Concentrating Solar Power
CRS	Central Receiver System
LCOE	Levelized Cost of Electricity ($€/MWh$)
TRNSYS	Transient System Simulation Tool
EES	Engineering Equation Solver
sCO ₂	Supercritical Carbon Dioxide
Gen3 CSP	Third-Generation Concentrating Solar Power
NREL	National Renewable Energy Laboratory
MCRT	Monte Carlo Ray Tracing

1 Introduction

Concentrating Solar Power (CSP) technologies are increasingly recognized for their ability to deliver dispatchable, low-carbon electricity. Among these, central receiver systems (CRS), also referred to as solar tower plants, achieve superior thermodynamic efficiency due to their capability to reach operating temperatures above 565 °C. The combination of a heliostat field and a high-temperature molten-salt receiver allows energy capture and storage for power generation during both on- and off-sun periods.

The optical performance of the heliostat field and receiver directly affects overall plant efficiency and levelized cost of electricity (LCOE). Loss mechanisms such as cosine error, blocking, shading, spillage, and atmospheric attenuation contribute significantly to energy deficits and therefore must be minimized during design optimization. Previous studies have provided important advances in this field. Augsburger (2013) developed a thermo-economic optimization framework for large-scale tower systems using TRNSYS-EES coupling, establishing relationships between solar multiple, receiver geometry, and storage capacity. De Meyer et al. (2016) proposed a one-dimensional thermal-resistance network for molten-salt receivers, offering a reliable approach to predict tube temperature distributions. More recently, Alfani et al. (2022) and Mehos et al. (2017) investigated next-generation systems integrating high-temperature receivers with supercritical carbon-dioxide (sCO₂) Brayton cycles. The Gen3 CSP Roadmap identifies this configuration as a

* Corresponding author: khalid.bouaiche-etu@etu.univh2c.ma

leading pathway to increase efficiency and lower costs, although the resulting LCOE remains scenario-dependent. In North Africa, Morocco presents favorable conditions for CSP development owing to its high annual Direct Normal Irradiance (DNI > 2400 kWh m⁻² year⁻¹) and vast arid land availability. For instance, the NOOR III solar tower in Ouarzazate reports a solar resource of 2508 kWh m⁻² year⁻¹ on the NREL SolarPACES database and operates with a 247 m tower and 7 h molten-salt storage. These conditions position Morocco among the most promising locations for further tower-based CSP deployment. Nevertheless, a systematic investigation of geometrical optimization under Moroccan climatic conditions has yet to be reported. The present study aims to address this gap by employing MCRT-based optical modeling to determine the optimal tower height and receiver geometry that maximize optical efficiency while maintaining realistic design constraints. Unlike previous studies that are limited to evaluating overall optical efficiency, this work focuses on analyzing in detail the impact of geometric parameters on each of the optical loss mechanisms, namely cosine losses, atmospheric attenuation, spillage losses, as well as blocking and shading. This approach makes it possible to clearly identify the influence of each design parameter on the different loss components for the site in question, and thus serves as a relevant tool for guiding system optimization according to local conditions.

2 Methodology

2.1 Site and data collection

The study site is located in southern Morocco, a region characterized by an arid climate, strong solar resource, and low atmospheric humidity. Meteorological data were collected from the Photovoltaic Geographical Information System (PVGIS) in Typical Meteorological Year (TMY) format. The dataset provides hourly values of DNI, ambient temperature, and wind speed, which were used as inputs for the simulation. The average annual DNI exceeds 2400 kWh m⁻² year⁻¹, comparable to that of Ouarzazate, where NOOR III operates.

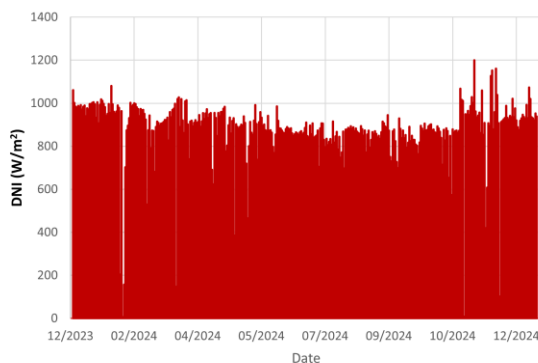


Fig. 1. Daily Direct Normal Irradiance (DNI)

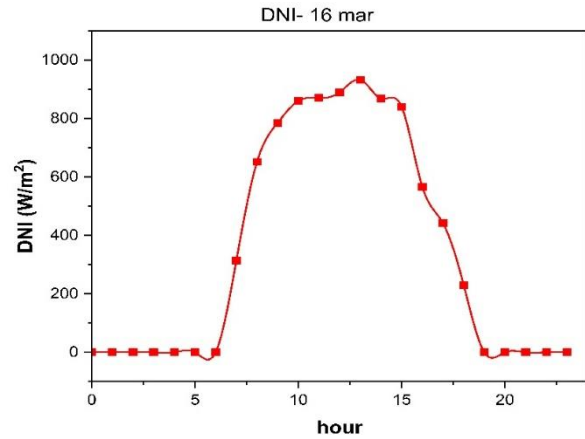


Fig. 2. Hourly DNI for 16 mars

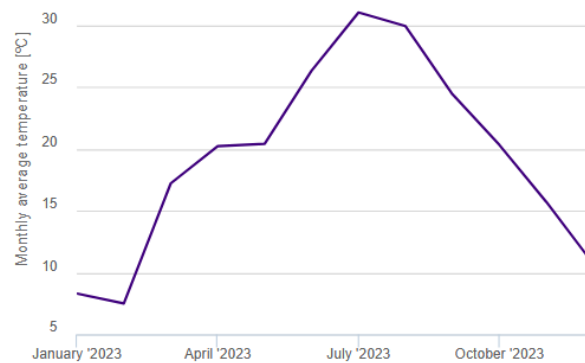


Fig. 3. Monthly average temperature.

2.2 Simulation framework

Optical modeling was performed using SolarPILOT (National Renewable Energy Laboratory, USA). The software integrates analytical field algorithms with the SolTrace Monte-Carlo ray-tracing engine to compute solar flux distributions on the receiver and quantify optical losses. The DelSol3 algorithm was used to generate a radial-staggered heliostat layout, and a limb-darkened solar model was applied to represent the non-uniform brightness of the solar disc. The receiver was assumed to be an external cylindrical molten-salt receiver. Mirror reflectivity and soiling efficiencies were both set to 0.95, and atmospheric attenuation was modeled as a function of optical path length and air transmittance.

The optical efficiency η_{opt} was determined from the product of the component efficiencies:

$$\eta_{opt} = \eta_{cos} \times \eta_{blk} \times \eta_{spl} \times \eta_{att} \quad (1)$$

where η_{cos} , η_{blk} , η_{spl} , and η_{att} denote efficiencies associated with the cosine effect, blocking/shading, spillage, and atmospheric attenuation, respectively.

2.3 Parametric study

A parametric analysis was conducted to evaluate the influence of geometric parameters on optical efficiency. Tower height was varied from 120 m to 240 m, receiver height from 15 m to 30 m, and receiver diameter from 10

m to 25 m. For each configuration, SolarPILOT automatically optimized heliostat count and field area to achieve maximum optical performance.

The variation ranges of the studied parameters were defined to cover both the values typically reported in the literature for industrial-scale solar tower plants and values that were deliberately slightly widened. Using broader margins allows for analyzing the response of the optical system beyond nominal conditions and for identifying the thresholds at which certain optical losses become dominant. Additionally, to strengthen the robustness of the conclusions by including slightly over- or underestimated cases, the analysis allows for verifying that the observed trends remain valid over a wider operating range than just the design point.

Table 1. Constant simulation parameters.

Parameter	Value	Parameter	Value
Mirror slop error in X and Y (rad)	0.00153	Reflective surface ratio	0.97
Reflected beam error in X and Y (rad)	0.0002	Receiver thermal absorbance	0.94
Mirror reflectivity	0.95		

The resulting efficiencies and loss distributions were analyzed to identify the configuration that minimized total optical losses while ensuring uniform flux distribution on the receiver surface.

3 Results and Discussion

While the field of heliostats concentrates the sun light on the cylindrical receiver in top of a central tower, different types of optical loss occur due related to geometrical parameters, atmospheric effects, and imperfections.

in this section, the geometrical parameters of tower, receiver and heliostats are analyzed to evaluate their influence on the optical performance of the system and to identify the appropriate compromise between parameters for maximal efficiency. Constant simulation parameters are provided in **Table 1**.

3.1 Effect of tower height on optical loss factors

The tower height is an important parameter that affects the capacity of a heliostat to reflect rays and redirect it to the receiver. That why it affects the total efficiency, field layout and heliostats count. The appropriate tower height selection is based on its effect on different optical losses factors, especially the cosine factor, shading and blocking, atmospheric attenuation and solar rays' interception at the receiver.

The analysis is carried out using a default receiver height and shape (External cylindrical receiver with a diameter of 17.65 meters and a height of 21.6 meters), heliostats shape, size and collision radius are taken (mirrors with 12.2 meters of length, 12.2 meters of width and 8.6 meters of heliostat collision radius) for this simulation step.

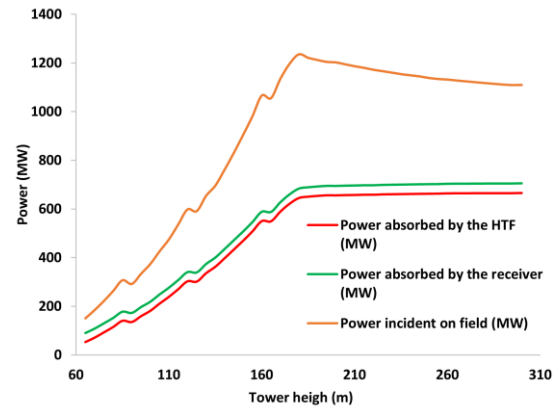


Fig. 4. Effect of tower height on received solar power.

The relation between the power absorbed by the receiver (Also by HTF) versus the tower optical height is shown for the current simulation stage. The optimum tower height is found to be about 180 meters, at which the power can be absorbed by the receiver is getting stable with very little growth. Also, a maximum count of heliostats (9005 heliostat) corresponds to a tower height of about 180 m.

In figure 4 the efficiency is calculated for different tower elevations.

The increasing of tower height impacts the angle between the heliostat normal and the sun's rays, for lower solar tower elevations, the heliostats close to the tower exhibit high angle of incidence, they must aim almost straight up, resulting in a large cosine loss making the mirrors reflective area inefficient. On the other hand, higher tower gives the heliostats in inner and middle regions of the field steeper aim point due to low incidence angle values which decreases cosine optical loss and increases their effectiveness.

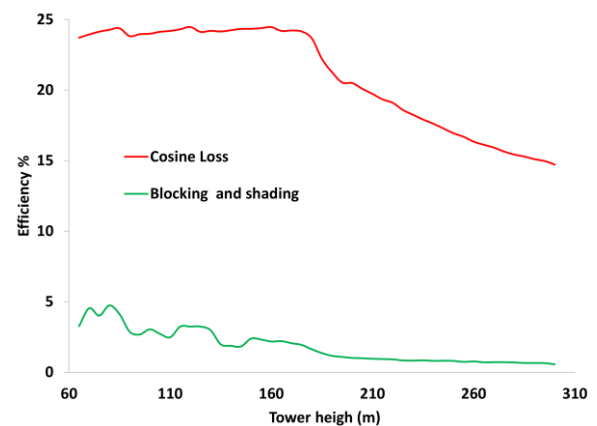


Fig. 5. Effect of tower height on Cosine, Blocking and Shading losses.

Figure 5 shows that the cosine optical loss decreases from about 24.47% to 20.50% while the tower height increases from 160 to 200 meter. Also, the blocking and

shading loss decreases due to the increase in tower height, which suggests that the interference between heliostats is reduced.

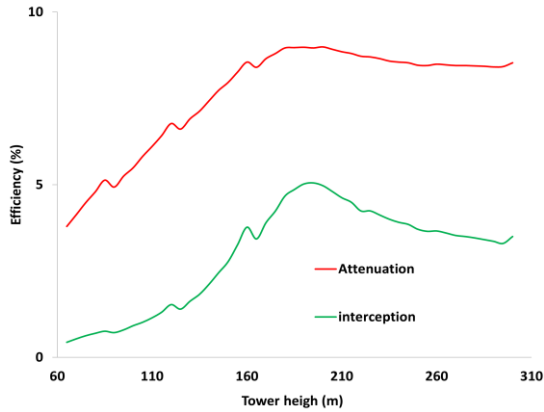


Fig. 6. Effect of tower height on interception and attenuation losses.

As the reflected solar beam from each mirror travels through the atmosphere toward the receiver, a part of solar energy gets absorbed and (or) scattered by air molecules, resulting in a reduction in solar radiation intensity. The absorbed energy fraction depends on the distance travelled by the solar ray. Figure 6 shows that the attenuation loss increases from about 4.79% to 8.85% as the tower height increases from 80 to 210 meters, due to the fact that for high tower heights the average path length becomes longer. Similarly, the interception loss increases with the increase of the solar receiver elevation, the figure shows that with the increment of solar tower height from about 65 to 195 meters, the portion of solar portion of reflected solar radiation from heliostats that is not captured by the receiver increases by about 5%.

3.2 Effect of heliostat shape and area

The effect of the heliostat geometry is evaluated by varying the surface area, also, the layout performances can be affected by changing the geometric parameters (structure width, and structure height) while keeping the surface area constant. However, each of these parameters has an effect on the layout shape and overall performance. Therefore, they must be adjusted simultaneously to determine the most suitable combination.

3.2.1 Square surface heliostat

Considering square-shaped heliostats, the effect of mirror reflective surface area on different optical losses and overall performance of the solar tower plant is investigated. While keeping other parameters constant, the main affected loss parameters by the heliostat surface area changing are shown in **Table 2**.

Table 2. Effect of heliostat solar area on the field loss factors and optical performance.

S (m ²)	1.00	400.00	Factor variation (%)
Cosine efficiency (%)	20.05	21.36	1.31
Blocking efficiency (%)	0.43	1.69	1.26
Image interception (%)	4.46	5.35	0.89
Field optical efficiency (%)	58.89	56.49	-2.40

When the heliostat surface area is increased from 1 to 400-meter square, even though the total simulated reflective area of the field increases, the field optical performance decreases by about 2.4% resulting in a reduction of the thermal power absorbed by the HTF by about 4.0MW.

3.2.2 Rectangular surface heliostat

The surface area of the heliostat is adjusted to simulate different width and length cases, for a fix heliostat area (175 m²).

Figure 7 shows the Effect of heliostat width and length on efficiency and field heliostat count.

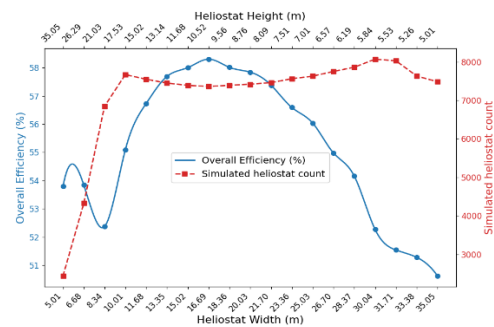


Fig. 7. Effect of heliostat width and length on efficiency and field heliostat count.

Efficiency peaks around 20 meters of width where the heliostat length is about 9 meters and the heliostat count is about 7400.

3.3 Effect of receiver area

As previously mentioned, each parametric related to the geometric design of the solar tower or that of heliostats has significant effect on one or more optical loss factors in the central receiver system, and therefore on the system global efficiency. The geometric design, shape and area, of the solar receiver have also a major effect on the overall efficiency and loss factors, especially the interception loss. This last occurs when a portion of the reflected solar radiation from the heliostat field misses the receiver due to imperfections and geometry limitations, resulting in a reduction of the overall optical efficiency. In this section, the effect of receiver diameter and height is evaluated.

The simulation is done for a tower height of 195 meters, 21.6 meters of receiver height with 175 m² of heliostat surface area.

3.3.1 Receiver diameter effect

The solar receiver main role is to absorb the solar radiations reflected through the heliostat field and convert it into thermal energy which will then be transferred, by the HTF, to the power bloc. This conversion of solar radiation into thermal energy represents more complexity at the receiver surface, due to the occurrence of various types of thermal losses, especially radiation and convection, which are proportional to the receiver surface area, such that the use of large small receivers reduces the effect of convection and radiation loss factors, but at the same time, it exhibits high interception losses, and vice versa.

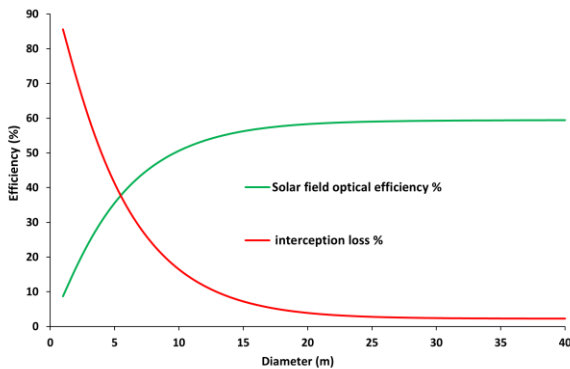


Fig. 8. Effect of receiver diameter on interception loss and overall efficiency

For small receiver diameters, the limited surface area of the receiver exhibits high solar flux density figure 9, however, a significant fraction of the reflected solar flux misses the receiver, which lead to an important interception loss, figure 8, and, consequently, lower overall optical efficiency.

Above 20 meters of diameter, the intercepted beam portion approaches zero, and the field efficiency becomes maximal.

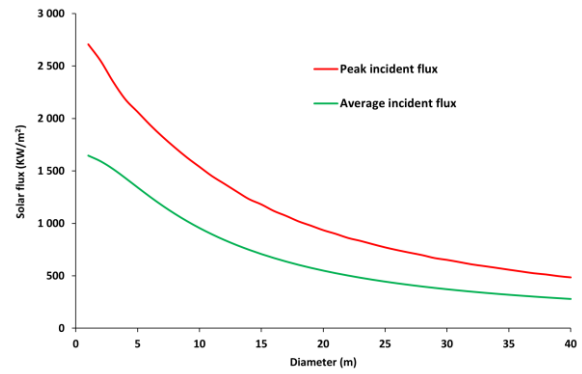


Fig. 9. Effect of receiver diameter on the received solar flux

3.3.2 Receiver height effect

In this part, previous solar field is used for the simulation, with 17.65 meters of receiver diameter, while the receiver height is adjusted from 10 to 35 meters.

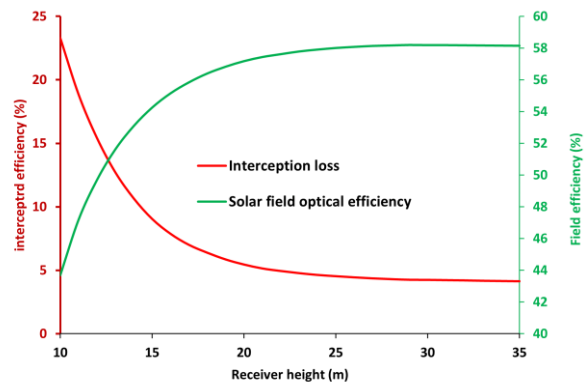


Fig. 10. Effect of receiver height on interception loss and optical efficiency

Figure 10 shows the influence of the receiver height on interception loss factor, so that for 10 meters of receiver height, about 23.3% of solar beam is intercepted, while at above 25 meters of height, the interception loss is reduced to below 5%.

3.4 Derivation of the Optimal Design

The main objective of this numerical simulation study is to investigate the optical efficiency and the different types of optical losses related to the various components of the solar plant in order to find a compromise between its geometric parameters and optical losses, which allows delivering maximum efficiency.

From the previous sections, the optimal configuration could be derived with a tower height of about 200 meters, a receiver diameter and height of about 17.65 and 21.6 meters respectively, with a square heliostat surface of about 149 m², and a default collision radius of 8.6 meters.

For this configuration, the optical efficiency of the solar plant becomes maximal, exceeding 61%, with a field of about 8700 heliostats. The radial scatter of the heliostat field is represented in figure 11.

The atmospheric attenuation and image interception loss factors are minimum with about 4.97% and 9% respectively, while the cosine and blockage losses are about 20.54% and 1% respectively.

The concentrated solar flux distribution on the cylindrical receiver is represented in figure 12.

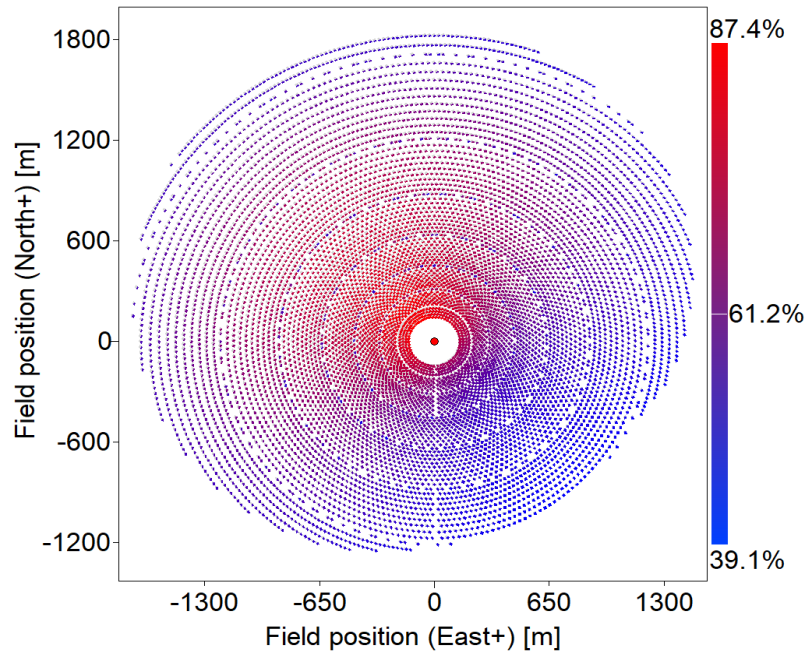


Fig. 11. Heliostat field.

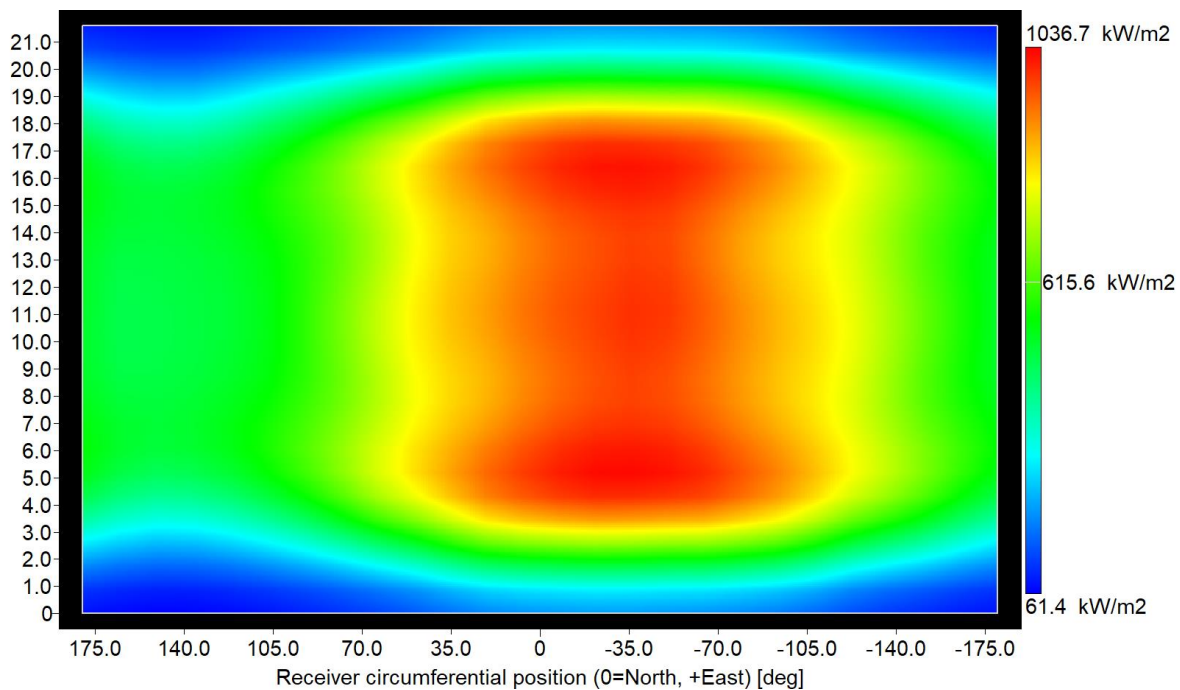


Fig. 12. Receiver solar flux distribution.

4 Conclusion

The present numerical investigation explored the effect of variation in geometrical parameters namely_ tower height, receiver dimensions, and heliostat configuration_ on the overall optical performance of a central receiver solar system located in southern Morocco. Results indicated that optimal performance of the studied solar plant is found for a tower height range of 180-200 m, yielded a total optical efficiency exceeding 60%. Different loss factors have been evaluated, where the cosine and atmospheric attenuation have major effect, while blocking and shading remained minimal.

References

1. M.J. Wagner, *Simulation and Predictive Performance Modeling of Utility-Scale Central Receiver System Power Plants*, Master's thesis, University of Wisconsin–Madison, Sandia National Laboratories (2008).
2. M.A. Ekkeri, U. Farooq, P. Partibhan, K. Thomas, *Concentrated Solar Power: Design of a CSP Tower Plant in NEOM (Saudi Arabia)*, Politecnico di Milano (2023). <https://doi.org/10.13140/RG.2.2.25588.42886>
3. G. Augsburger, *Thermo-Economic Optimisation of Large Solar Tower Power Plants*, Ph.D. thesis, École Polytechnique Fédérale de Lausanne (EPFL) (2013).
4. O.A.J. de Meyer, F. Dinter, S. Govender, “Thermal Resistance Model for CSP Central Receivers.” *AIP Conf. Proc.*, **1734**, 030010 (2016). <https://doi.org/10.1063/1.4949062>
5. *Flow Patterns of External Solar Receivers: Experimental and CFD Study of Air-Receiver Flow Distribution and Flux Uniformity*, unpublished report.
6. A.S. Pidaparathi, F. Duvenhage, J. Hoffmann, *A Parametric Study of Heliostat Size for Reductions in Levelized Cost of Electricity*, Stellenbosch University, South Africa (2016).
7. G. Zhu, P. Kumar, M. Wolf, et al., *Roadmap to Advance Heliostat Technologies for Concentrating Solar-Thermal Power*, NREL/TP-5700-83041, Golden, CO (2022).
8. National Renewable Energy Laboratory, *Cost Update: Commercial and Advanced Heliostat Collectors*, NREL Technical Memo (2021).
9. Lafayette Energy Systems, *Drop C: The Drop-In “Ring-of-Power” Heliostat*, White Paper (2020).
10. J. Gómez-Hernández, P.A. González-Gómez, J.V. Briongos, D. Santana, “Maximizing the Power-Block Efficiency of Solar Tower Plants: Dual-Pressure Level Steam Generator.” *Appl. Therm. Eng.*, **144**, 583–592 (2018). <https://doi.org/10.1016/j.applthermaleng.2018.08.054>
11. D. Alfani, T. Neises, M. Astolfi, M. Binotti, P. Silva, “Techno-Economic Analysis of CSP Incorporating sCO₂ Brayton Power Cycles: Trade-Off Between Cost and Performance.” *AIP Conf. Proc.*, **2445**, 090001 (2022). <https://doi.org/10.1063/5.0086353>
12. Black & Veatch, *Molten Salt Concept Definition and Capital Cost Estimate*, DOE SunShot Report (2016).
13. C.S. Turchi, G.A. Heath, *Molten Salt Power Tower Cost Model for the System Advisor Model (SAM)*, NREL/TP-5500-57625, Golden, CO (2013).
14. S. Ladkany, W. Culbreth, N. Loyd, “565 °C Molten Salt Solar Energy Storage Design, Corrosion, and Insulation.” *J. Energy Power Eng.*, **12**, 517–532 (2018).
15. J. Schulte-Fischedick, R. Tamme, U. Herrmann, “CFD Analysis of the Cool-Down Behaviour of Molten Salt Thermal Storage Systems.” *ASME Energy Sustain. Conf. Proc.*, Paper ES2008-54101 (2008).
16. K.R. Gautam, M.A. Bashir, G. Frate, “Review and Techno-Economic Analysis of Emerging Thermo-Mechanical Energy Storage Technologies.” *Energies*, **15**, 6328 (2022). <https://doi.org/10.3390/en15176328>
17. U.S. Department of Energy, *Developing a Cost Model and Technology to Estimate Capital Costs for Thermal Energy Storage*, DOE Report (2019).
18. Sandia National Laboratories, *Advanced Thermal Storage for Central Receivers with Supercritical Coolants* (2020).
19. International Renewable Energy Agency (IRENA), *Renewable Energy Cost Analysis: Concentrating Solar Power*, Abu Dhabi (2012).
20. U.S. Energy Information Administration (EIA), *Capital Cost and Performance Characteristics for Utility-Scale Electric Power Generating Technologies*, Sargent & Lundy Report 14987.001 (2024).
21. L. Wang, et al., *Analysis of the Cost and Value of Concentrating Solar Power in China*, NREL/IEA Study (2022).
22. U.S. Bureau of Labor Statistics, *Producer Price Index (PPI) Report – November 2024*, Washington, DC (2024).
23. R. Kumar, V.P. Singh, A. Kumar, “Thermal Performance and Economic Analysis of a 210 MWe Coal-Fired Power Plant.” *J. Thermodyn.*, **2014**, Article ID 520183 (2014). <https://doi.org/10.1155/2014/520183>
24. NOOR III CSP Project (Ouarzazate, Morocco), *NREL SolarPACES Database* (2022). 247 m tower, 150 MW_e, 7 h TES, LCOE ≈ 0.15 USD kWh⁻¹.
25. Crescent Dunes Solar Energy Project (Nevada, USA), *NREL SolarPACES Database* (2023). 110 MW_e, 195 m tower, 10 h TES, LCOE ≈ 0.18 USD kWh⁻¹.
26. Atacama I / Cerro Dominador (Calama, Chile), *NREL SolarPACES Database* (2023). 110 MW_e CSP + 100 MW_e PV hybrid; 17.5 h TES; LCOE ≈ 0.10 USD kWh⁻¹.
27. Shouhang Dunhuang Phase II Tower (China), *NREL SolarPACES Database* (2022). 100 MW_e, 263 m tower, 11 h TES, LCOE ≈ 0.08 USD kWh⁻¹.
28. M. Mehos, C. Turchi, J. Vidal, M. Wagner, Z. Ma, *Concentrating Solar Power Gen3 Demonstration Roadmap*, NREL/TP-5500-67464, Golden, CO (2017).
29. M.N. Saeed, N. Rüsche, H. Dieringer, “Production of Aviation Fuel with Negative Emissions via Chemical Looping Gasification of Biogenic Residues: Full Chain Process Modelling and Techno-Economic Analysis.” *Fuel Process. Technol.*, **241**, 107585 (2023). <https://doi.org/10.1016/j.fuproc.2023.107585>